Deposition of Molybdenum Oxide Thin Films on Silicon Substrates for High-Performance Transparent Electronics

Mehmet N. Abdullah

Department of Electric and Electronic Engineering, Faculty of Engineering, Middle East Technical University, Ankara, TÜRKIYE
Email: mohammedhameed701@yahoo.com

Abstract
This letter demonstrates the successful atomic layer deposition (ALD) of molybdenum oxide (MoO_3) thin films on silicon substrates for high-performance transparent electronics. The films were characterized using current density-voltage (J-V) and capacitance-voltage (C-V) measurements, which confirmed the formation of a high-quality Schottky junction. The Ag/MoO_3/n-Si heterostructure exhibited excellent rectification, with a ratio of ~870, an ideality factor of 1.8, and a built-in potential of 0.68 eV. These results underscore the potential of ALD-grown MoO_3 as a superior hole-injection layer, enabling efficient charge transport in next-generation optoelectronic devices.

Keywords: Molybdenum oxide; Thin films; Atomic layer deposition; Transparent electronics
Received: October 2025; **Revised:** December 2025; **Accepted:** December 2025; **Published:** January 2026

1. Introduction

High-performance transparent electronics represent a frontier in modern technology, merging optical transparency with robust electrical functionality. These systems, characterized by high visible-light transmittance and excellent electrical conductivity, are typically fabricated from wide-bandgap semiconductors and transparent conductive oxides like ITO, or emerging materials such as graphene and silver nanowires [1-4]. Advanced deposition techniques, including sputtering and printing, enable their preparation on flexible substrates. Their unique synergy of properties unlocks transformative applications, including next-generation displays, transparent solar cells, smart windows, and wearable biosensors, driving innovation across consumer electronics, energy, and healthcare by seamlessly integrating electronic intelligence into our visual environment [5-8].

Molybdenum oxide thin films, particularly its sub-stoichiometric (MoO_{3-x}) and fully oxidized (MoO_3) phases, exhibit a unique combination of physical and chemical properties crucial for advanced devices, including high chemical stability, wide bandgap (2.8–3.6 eV), and intriguing optoelectronic characteristics like n-type/p-type conductivity and electrochromism. These films are typically prepared via techniques such as sputtering, thermal evaporation, and atomic layer deposition, allowing precise control over stoichiometry and morphology [9-12]. Leveraging these properties, they find extensive applications as hole/electron transport layers in organic photovoltaics and LEDs, as active electrodes in supercapacitors and smart windows, and as sensitive gas sensors, underscoring their versatility in modern electronics and optoelectronics [13-17].

Atomic Layer Deposition (ALD) has emerged as a premier technique for the fabrication of ultra-thin, conformal, and pinhole-free films, distinguished by its unique, self-limiting surface reactions. This vapor-phase deposition method relies on the sequential and cyclic exposure of a substrate to precursor vapors, separated by purging intervals, enabling precise sub-nanometer control over film thickness and exceptional uniformity across complex, high-aspect-ratio structures [18,19]. The application of ALD for synthesizing metal oxide thin films is particularly significant, leveraging precursors such as metal halides, alkyls, or alkoxides, which react with co-reactants like water, ozone, or oxygen plasma. This process facilitates the growth of a wide portfolio of functional oxides—from dielectrics like Al_2O_3 and HfO_2 to semiconductors like ZnO and TiO_2, and conducting oxides like ITO—with tailored stoichiometry and minimal defect densities [20,21]. The self-limiting mechanism ensures unparalleled conformality, making ALD indispensable for coating intricate nanostructures and porous materials where other techniques fail. Consequently, ALD-grown metal oxide films are foundational to numerous cutting-edge technologies, serving as high-κ gate dielectrics in nanoelectronics, protective layers in energy storage devices, catalytic coatings in reactors, and active components in sensors and optoelectronic devices [22-24]. The unparalleled control, versatility, and scalability of ALD firmly establish it as a

cornerstone technology for advancing modern materials science and nano-fabrication [25-27].

2. Experimental Part

The atomic layer deposition (ALD) of molybdenum oxide thin films was conducted in a commercially available, hot-wall, flow-type ALD reactor. The system featured a sealed stainless-steel reaction chamber capable of maintaining a base vacuum better than 10^{-2} mTorr, ensured by a combination of a turbomolecular and a scroll dry pump. A rectangular, native-oxide-covered silicon (100) wafer, cleaved into approximately 1 cm x 1 cm pieces, was used as the substrate. These substrates were meticulously cleaned prior to deposition through a standard RCA protocol, followed by a 60-second dip in a dilute hydrofluoric acid (HF) solution to remove the native oxide and create a hydrogen-terminated surface, thereby ensuring a clean and reactive starting interface for uniform film nucleation. The substrates were then loaded onto a ceramic boat and placed inside the central, heated zone of the reactor chamber. Precise temperature control was critical; the chamber walls and the precursor delivery lines were heated to 110°C to prevent precursor condensation, while the substrate holder temperature was independently controlled and maintained at a constant growth temperature of 200°C for all experiments, a value optimized to provide sufficient thermal energy for surface reactions while avoiding undesirable thermal decomposition of the precursors.

The deposition process utilized molybdenum hexacarbonyl ($Mo(CO)_6$, 99.9% purity) as the metal precursor and ozone (O_3) as the co-reactant. The $Mo(CO)_6$ solid source was contained in a stainless-steel bubbler, which was heated to 50 °C using a proportional-integral-derivative (PID)-controlled heating jacket to generate a sufficient vapor pressure. High-purity nitrogen (N_2, 99.99%) gas, further purified by an inline gas purifier, was used as both the carrier and purging gas, with a continuous flow rate maintained at 200 sccm. A single ALD cycle consisted of four distinct steps: (1) a $Mo(CO)_6$ precursor pulse, typically between 1-3 seconds, delivered by passing the N_2 carrier gas through the bubbler; (2) a 30-second N_2 purge to remove all non-reacted precursor molecules and any gaseous by-products from the chamber; (3) an O_3 pulse of 5 seconds, generated in-situ from oxygen gas by a commercial ozone generator with a concentration of approximately 200 g/N.m³; and (4) a final 40-second N_2 purge to evacuate any excess O_3 and reaction by-products before commencing the next cycle. This sequence - $Mo(CO)_6$ pulse / N_2 purge / O_3 pulse / N_2 purge - constituted one ALD cycle, with the number of cycles (e.g., 100 to 500) being precisely controlled to achieve the target film thickness. The self-limiting nature of the reaction was verified through saturation studies, where the pulse times of both precursors were varied independently to confirm that the growth per cycle (GPC) reached a constant plateau, a hallmark of a true ALD mechanism. Figure (1) shows a schematic diagram of the experimental part of this work while figure (2) shows the deposition rate of the MoO_3 thin films prepared in this work.

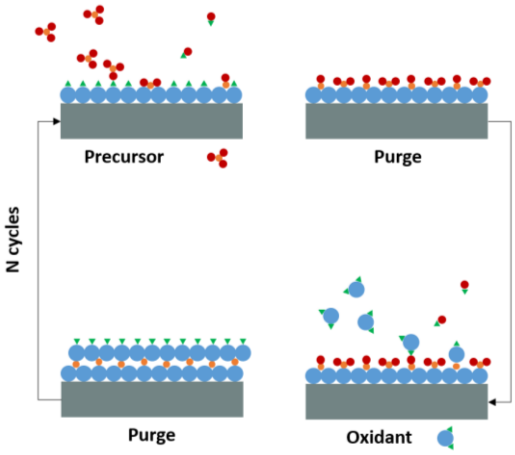

Fig. (1) Schematic diagram of the experimental part of this work

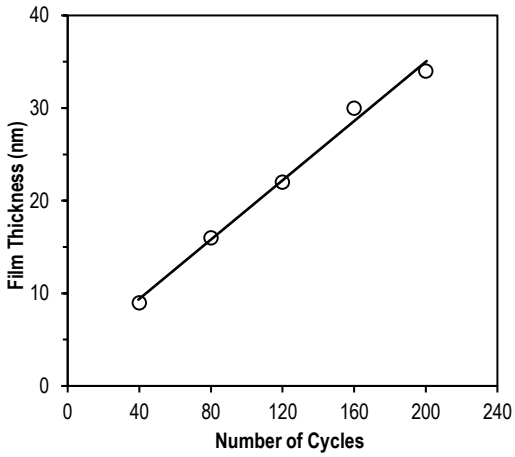

Fig. (2) The deposition rate of MoO_3 thin films

3. Results and Discussion

The rectification ratio of a diode is the ratio of the current at a specified forward voltage to the current at the same magnitude of reverse voltage. At 2.0 V, forward current density (J_f) = 1.48 x 10^{-2} A/cm², reverse current density (J_r) = -1.70 x 10^{-5} A/cm², and the rectification ratio = ($|J_f/J_r|$) = $|1.48 \times 10^{-2} / 1.70 \times 10^{-5}| \approx 870$. A rectification ratio of nearly three orders of magnitude is excellent and confirms the high quality of the ALD film and the well-defined Schottky junction.

The ideality factor (n) can be estimated from the slope of the linear region of the ln(J)-V plot (Fig. 3) in forward bias (e.g., between 1.0 V and 1.6 V). Using the standard thermionic emission equation:

$$J = J_s\left[\exp\left(\frac{qV}{nk_BT}\right) - 1\right] \quad (1)$$

where J_s is the saturation current, which can be extrapolated from the ln(J) vs. V plot to V=0. From the data trend, J_s is approximately 1.0×10^{-9} A/cm². The slope in the mentioned region gives an ideality factor of n ≈ 1.8. This value, greater than 1, indicates deviations from ideal thermionic emission, likely due to interface states, recombination in the depletion region, or the impact of the thin oxide film itself.

The Schottky barrier height (Φ_B) can be calculated from (J_s) using the relationship $J_s = A^*T^2 \exp(-q\Phi_B/k_BT)$, where A* is the Richardson constant. Assuming A* = 112 A/cm²/K² for n-Si and T = 300 K, $\Phi_B=(k_BT/q)\ln(A^*T^2/J_s) \sim 0.83$ eV. This significant barrier height is consistent with the high work function of MoO_x and explains the strong rectifying behavior and low reverse leakage current observed in the data.

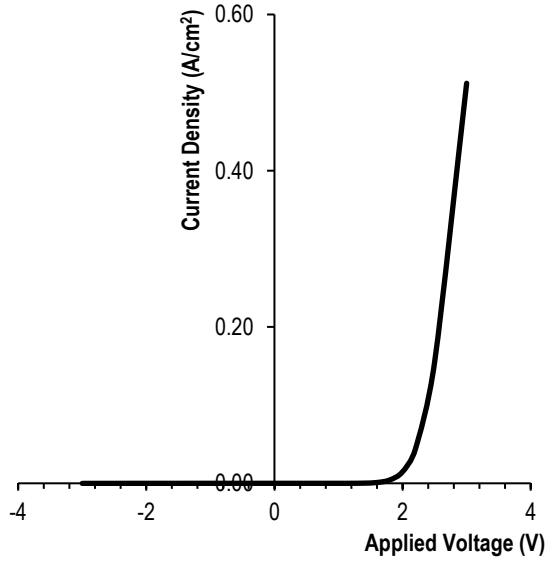

Fig. (3) The J-V characteristics of the MoO_3/Si heterojunction prepared in this work

The C-V characteristics provide crucial information about the electronic properties of the MoO_x/n-Si heterojunction, complementing the J-V analysis. The C-V plot (Fig. 4) shows a classic response for a Schottky junction on a semiconductor. In reverse bias (< 0 V), the capacitance is low and decreases slowly with increasing reverse bias. This corresponds to the widening of the depletion region in the n-Si substrate. The MoO_x layer itself acts as a dielectric in series with the semiconductor depletion capacitance. In forward bias (> 0 V), the capacitance increases sharply near ~0.7 V. This is the onset of strong forward injection, where the depletion region collapses, and the measured capacitance is dominated by the diffusion capacitance of injected minority carriers and the geometric capacitance of the thin MoO_x layer. The rapid rise prevents accurate measurement beyond this point, indicating the built-in potential of the junction.

The Mott-Schottky plot ($1/C^2$ vs. V) is linear in the reverse bias region (-3.0 V to ~0 V), confirming the formation of a Schottky barrier and allowing for quantitative parameter extraction. Using the Mott-Schottky relationship for an n-type semiconductor:

$$\frac{1}{C^2} = \frac{2}{q\varepsilon_r\varepsilon_0 N_d}\left(V_{bi} - V - \frac{k_BT}{q}\right) \quad (2)$$

where ε_r and ε_0 are the relative and vacuum permittivities, respectively, N_d is the donor density in the n-Si substrate, and V_{bi} is the built-in potential. Accordingly, $N_d = 2.0\times10^{15}$ cm^{-3}, which is typical for a moderately doped n-type silicon substrate

The C-V data and its analysis confirm the formation of a high-quality Schottky junction. The linear Mott-Schottky plot indicates a uniform donor density, and the extracted built-in potential aligns with the expected band alignment between MoO_x and n-Si. Together with the J-V data, this provides a comprehensive electrical characterization, demonstrating that the ALD MoO_x film forms a well-defined, electronically stable interface with silicon, which is critical for its reliable operation in optoelectronic devices.

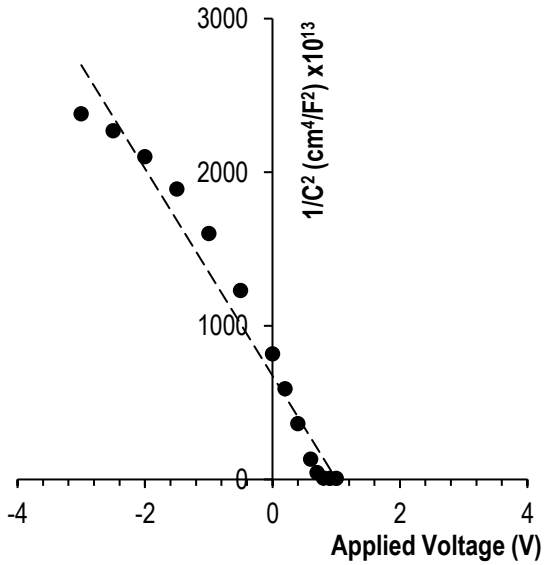

Fig. (4) The C-V characteristics of the MoO_3/Si heterojunction in both forward and reverse biasing conditions

4. Conclusions

Successful atomic layer deposition (ALD) of molybdenum oxide (MoO_3) thin films on silicon substrates for high-performance transparent electronics was presented. The results confirmed the formation of a high-quality Schottky junction. The Ag/MoO_3/n-Si heterostructure exhibited excellent rectification, with a ratio of ~870, an ideality factor of 1.8, and a built-in potential of 0.68 eV. These results underscore the potential of ALD-grown MoO_3 as a superior hole-injection layer, enabling efficient

charge transport in next-generation optoelectronic devices.

References

[1] O. Stroyuk et al., "Atomically thin 2D materials for solution-processable emerging photovoltaics", *Chem. Commun.*, 61(3) (2024) 455-475.

[2] A. Sharif et al., "The role of fluence in determining the response of thin molybdenum films to ultrashort laser irradiation; from laser-induced crystallization to ablation via photomechanical ablation and nanostructure formation", *Appl. Surf. Sci.*, 592 (2022) 153315.

[3] J. Park, M. Shin and J. Yi, "Comparative study of aluminum and nickel contact electrodes for indium–tin–zinc oxide thin film transistors using oxygen vacancy diffusion model", *Mater. Sci. Semicond. Process.*, 120 (2020) 105253.

[4] E. Lamanna et al., "Mechanically Stacked, Two-Terminal Graphene-Based Perovskite/Silicon Tandem Solar Cell with Efficiency over 26%", *Joule*, 4(4) (2020) 865-881.

[5] D.M. Torres-Herrera et al., "Thermal co-evaporated MoOx:Au thin films and its application as anode modifier in perovskite solar cells", *Sol. Ener.*, 206 (2020) 136-144.

[6] C.-C. Wu, "Ultra-high transparent sandwich structure with a silicon dioxide passivation layer prepared on a colorless polyimide substrate for a flexible capacitive touch screen panel", *Sol. Ener. Mater. Solar Cells*, 207 (2020) 110350.

[7] M.E. Sánchez Vergara et al., "Structural determination, characterization and computational studies of doped semiconductors base silicon phthalocyanine dihydroxide and dienynoic acids", *Heliyon*, 10(3) (2024) e25518.

[8] J.-C. Wang et al., "Enhanced field emission characteristics of WS_2 nano-films by diamond film and Mo film", *Vacuum*, 225 (2024) 113223.

[9] S. Jiang et al., "Indium-free flexible perovskite solar cells with AZO/Cu/Ag/AZO multilayer transparent electrodes", *Sol. Ener. Mater. Solar Cells*, 246 (2022) 111895.

[10] A. Kumar Singh et al., "Wafer-scale synthesis of two-dimensional ultrathin films", *Chem. Commun.*, 60(3) (2024) 265-279.

[11] Md. Hasnat Rabbi et al., "Growth of high quality polycrystalline InGaO thin films by spray pyrolysis for coplanar thin-film transistors on polyimide substrate", *J. Alloys Comp.*, 1002 (2024) 175203.

[12] K. Savkin et al., "Synthesis of magnesium oxide and zinc oxide powders in a glow discharge plasma at atmospheric pressure", *Ceram. Int.*, 50(5) (2024) 8185-8197.

[13] P.H. Nguyen et al., "Synergistic hole-doping on ultrathin MoTe2 for highly stable unipolar field-effect transistor", *Appl. Surf. Sci.*, 596 (2022) 153567.

[14] T. Maji et al., "One-layer water vapor poly(olefin) barriers compete metal sputtering onto flexible substrates", *Polymer*, 197 (2020) 122487.

[15] T. Hellmann et al., "Preparation and characterization of polythiophene/gold nanoparticles/carbon nanotubes nanocomposites thin films: Spectroscopy and morphology", *Mater. Today Commun.*, 33 (2022) 104314.

[16] O.A. Hammadi, M.K. Khalaf and F.J. Kadhim, "Fabrication of UV Photodetector from Nickel Oxide Nanoparticles Deposited on Silicon Substrate by Closed-Field Unbalanced Dual Magnetron Sputtering Techniques", *Opt. Quantum Electron.*, 47(12) (2015) 3805-3813.

[17] R.H. Turki and M.A. Hameed, "Spectral and Electrical Characteristics of Nanostructured NiO/TiO_2 Heterojunction Fabricated by DC Reactive Magnetron Sputtering", *Iraqi J. Appl. Phys.*, 16(3) (2020) 39-42.

[18] D. Gupta et al., "Defects engineering and enhancement in optical and structural properties of 2D-MoS_2 thin films by high energy ion beam irradiation", *Mater. Chem. Phys.*, 276 (2022) 125422.

[19] E. Butanovs et al., "The role of Al_2O_3 interlayer in the synthesis of $ZnS/Al_2O_3/MoS_2$ core-shell nanowires", *J. Alloys Comp.*, 918 (2022) 165648.

[20] F. Giannazzo et al., "Integration of graphene and MoS_2 on silicon carbide: Materials science challenges and novel devices", *Mater. Sci. Semicond. Process.*, 174 (2024) 108220.

[21] A.J. Santos et al., "Application of advanced (S)TEM methods for the study of nanostructured porous functional surfaces: A few working examples", *Mater. Character.*, 185 (2022) 111741.

[22] S. Sim et al., "Red and green inverted top-emitting quantum dot light-emitting diodes using CMOS-based electrodes for microdisplay applications", *Opt. Mater.*, 154 (2024) 115637.

[23] Md. Anower Hossain et al., "Atomic layer deposition enabling higher efficiency solar cells: A review", *Nano Mater. Sci.*, 2(3) (2020) 204-226.

[24] X. Zhou et al., "Reactively-sputtered AlO_x passivation layer for self-aligned top-gate amorphous InGaZnO thin-film transistors", *Mater. Sci. Semicond. Process.*, 148 (2022) 106796.

[25] Y. Choi et al., "Active pixel image sensor array based on large-scale ReS_2 semiconducting film", *Mater. Sci. Semicond. Process.*, 179 (2024) 108474.

[26] T. Wu et al., "Dual side transparent organic light-emitting diodes with a modified Ag top cathode", *Displays*, 83 (2024) 102713.

[27] T. Akila et al., "Augmented photovoltaic performance of Cu/Ce-(Sn:Cd)/n-Si Schottky barrier diode utilizing dual-doped Ce-(Sn:Cd) thin films", *Opt. Mater.*, 149 (2024) 115133.

